

Relieving the Tension between Weak Lensing and Cosmic Microwave Background with Interacting Dark Matter and Dark Energy Models

Rui An,^{1,*} Chang Feng,^{2,†} and Bin Wang^{3,1,‡}

¹*IFSA Collaborative Innovation Center, School of Physics and Astronomy,
Shanghai Jiao Tong University, Shanghai 200240, China*

²*Department of Physics, University of Illinois at Urbana-Champaign, 1110 W Green St, Urbana, IL, 61801, USA*

³*Center for Gravitation and Cosmology, College of Physical Science
and Technology, Yangzhou University, Yangzhou 225009, China*

We constrain interacting dark matter and dark energy (IDMDE) models using a 450-degree-square cosmic shear data from the Kilo Degree Survey (KiDS) and the angular power spectra from Planck’s latest cosmic microwave background measurements. We revisit the discordance problem in the standard Lambda cold dark matter (Λ CDM) model between weak lensing and Planck datasets and extend the discussion by introducing interacting dark sectors. The IDMDE models are found to be able to alleviate the discordance between KiDS and Planck as previously inferred from the Λ CDM model, and moderately favored by a combination of the two datasets.

PACS numbers:

I. INTRODUCTION

Cosmic shear, measured from distorted images of distant galaxies, can effectively map a three-dimensional dark matter structure in the late universe, making it a sensitive probe to constraining cosmological models. Recently, the standard Lambda cold dark matter (Λ CDM) model was examined by employing weak lensing data taken from a 450-deg² observing field of the Kilo Degree Survey (KiDS) [1] and it was disclosed that there exists a “substantial discordance” inferred from the Λ CDM model between the KiDS data [1–4] and the Planck 2015 cosmic microwave background (CMB) data [5, 6]. The discordance is at the level of 2.3σ and it was argued that this discordance can not be resolved even after reducing systematic uncertainties [1, 7]. In addition to the Λ CDM discordance between the KiDS and Planck datasets, earlier similar tension was also found to be substantial between the Canada-France-Hawaii Telescope Lensing Survey (CFHTLenS) [8–11] and Planck datasets [5, 12–15].

Besides the weak lensing–CMB discordance, the standard Λ CDM model is also challenged by other observations. There is approximately a 3σ tension in cosmological parameter space when the Λ CDM model is compared to Planck CMB data and local measurements of the Hubble constant based on the cosmic distance ladder [16, 17]. Recently, the Baryon Oscillation Spectroscopic Survey (BOSS) experiment of the Sloan Digital Sky Survey (SDSS) showed new evidence against the standard Λ CDM model [18] using measured baryon acoustic oscillations (BAO) in flux correlation functions of the Lyman- α forest from 158, 401 quasars at high redshifts ($2.1 \leq z \leq 3.5$). The results indicate a 2.5σ de-

viation from Λ CDM in the measurements of the Hubble constant and angular distance at an average redshift $z = 2.34$.

The tensions between observations of large-scale structure and CMB measurements made by Planck motivated a lot of studies to extend the standard Λ CDM model. So far the weak lensing data from KiDS have been used to test the extended cosmological models, which include massive neutrinos, nonzero curvature, evolving dark energy, modified gravity and running of the scalar spectral index [7]. It was found that the discordance between KiDS and Planck can be alleviated by introducing an evolving dark energy equation of state. Also, the CFHTLenS-Planck discordance has been revisited by using the extended models with a sterile neutrino and scale-dependent equation of state [14, 19]. Again, it was found that the confidence contours between two datasets started to overlap, effectively relieving the discordance. For the discordance between local Hubble constant and Planck measurements, a model with nonstandard physics in dark energy and dark radiation sectors was proposed to relieve the tension [17, 20, 21]. Similarly, it was suggested that an extended model with dark sectors’ interactions might be a solution to the discordance between the Hubble constant and the angular distance of BOSS at redshift $z = 2.34$ [22].

Not only being challenged by observations, the standard Λ CDM model is also suffering theoretical problems, such as the cosmological constant problem [23], i.e., a disagreement between the observed value and the estimation of quantum field theory. Moreover, the cosmological constant of the Λ CDM model can not explain why dark energy dominated evolution in the late universe, making a coincidence problem [24]. Given the fact that energy density fractions of dark matter and dark energy account for nearly 25% and 70% of the energy content of our universe, it is quite counter-intuitive to conceive that dark matter and dark energy co-exist independently in the course of cosmological evolution. From perspec-

*Electronic address: an_rui@sjtu.edu.cn

†Electronic address: changf@illinois.edu

‡Electronic address: wang_b@sjtu.edu.cn; Corresponding Author

tive of field theory, it is more natural to consider that there are interactions between dark matter and dark energy through either exotic energy or momentum transfer. And it was argued that a suitable amount of interactions between dark sectors can help alleviate the coincidence problem [22, 25–29]. Recently the models with interactions between dark sectors have been extensively tested with different observational datasets, such as measurements of the CMB and galaxy clusters, see the recent review [30] and references therein for detailed descriptions of physical models and observations.

In this work, we will constrain the interacting dark matter and dark energy model (IDMDE) using the weak gravitational lensing data from KiDS and Planck CMB data from both temperature and polarization. Moreover, we will revisit the discordance problem between KiDS and Planck with the IDMDE model and check if it is favored as compared to the standard Λ CDM model, and to what extent the tension would be relieved.

The paper is organized as follows. In Section II we introduce phenomenological models on the interactions between dark matter and dark energy with background dynamics equations and linear perturbations. In Section III we describe the KiDS measurements and statistical algorithms that are used to quantify tensions between different data sets. In Section IV we compare predicted weak lensing tomographic band powers from the IDMDE models to the KiDS-450 and Planck2015 datasets, and examine how the IDMDE models are favored by both KiDS and Planck data sets, and to what extent they alleviate the previous Λ CDM discordance problem. Finally, we discuss our results and conclude in Section V.

II. INTERACTING DARK MATTER AND DARK ENERGY MODELS

In this section, we begin with the phenomenological interacting dark matter and dark energy models [30] in the spatially flat Friedmann-Lemaître-Robertson-Walker (FLRW) universe. In these models, the total energy density of dark sectors is conserved and energy densities of dark matter and dark energy evolve individually as

$$\dot{\rho}_c + 3\mathcal{H}\rho_c = aQ, \quad (1)$$

$$\dot{\rho}_d + 3\mathcal{H}(1+w)\rho_d = -aQ, \quad (2)$$

where \mathcal{H} is the time-dependent Hubble constant defined by $\mathcal{H} = \dot{a}/a = aH$, a is the scale factor, the dot $\dot{}$ is the derivative with respect to conformal time, and $w = P_d/\rho_d$ is the equation of state of dark energy. Here Q denotes the interactions between dark sectors and it can be phenomenologically expressed as a linear combination of energy densities of dark matter and dark energy, i.e., $Q = 3\lambda_1 H\rho_c + 3\lambda_2 H\rho_d$ with λ_1 and λ_2 being free parameters describing interaction strength. In Table I, we list all of the phenomenological IDMDE models in which curvature perturbations are not divergent when conditions given by the last column are satisfied [31, 32].

TABLE I: Phenomenological interacting dark matter and dark energy models

Model	Q	w	Constraints
I	$3\lambda_2 H\rho_d$	$-1 < w < -1/3$	$\lambda_2 < 0$
II	$3\lambda_2 H\rho_d$	$w < -1$	$0 < \lambda_2 < -2w\Omega_c$
III	$3\lambda_1 H\rho_c$	$w < -1$	$0 < \lambda_1 < -w/4$
IV	$3\lambda H(\rho_c + \rho_d)$	$w < -1$	$0 < \lambda < -w/4$

In the linear theory, equations of the first-order perturbations for dark matter and dark energy are given by [33]

$$\dot{\delta}_c = -\left(kv_c + \frac{\dot{h}}{2}\right) + 3\mathcal{H}\lambda_2 \frac{1}{\mathcal{R}}(\delta_d - \delta_c), \quad (3)$$

$$\begin{aligned} \dot{\delta}_d = & -(1+w)(kv_d + \frac{\dot{h}}{2}) + 3\mathcal{H}(w - c_e^2)\delta_d \\ & + 3\mathcal{H}\lambda_1 \mathcal{R}(\delta_d - \delta_c) \\ & - 3\mathcal{H}(c_e^2 - c_a^2)[3\mathcal{H}(1+w) + 3\mathcal{H}(\lambda_1 \mathcal{R} + \lambda_2)] \frac{v_d}{k}, \end{aligned} \quad (4)$$

$$\dot{v}_c = -\mathcal{H}v_c - 3\mathcal{H}\left(\lambda_1 + \frac{1}{\mathcal{R}}\lambda_2\right)v_c, \quad (5)$$

$$\begin{aligned} \dot{v}_d = & -\mathcal{H}(1 - 3c_e^2)v_d \\ & + \frac{3\mathcal{H}}{1+w}(1 + c_e^2)(\lambda_1 r + \lambda_2)v_d + \frac{kc_e^2}{1+w}, \end{aligned} \quad (6)$$

where $\delta_i = \delta\rho_i/\rho_i$ is the perturbed density contrast, v_i is the peculiar velocity, and the subscript i represents dark matter or dark energy. The variable $h = 6\Theta$ is the synchronous gauge metric perturbation, Θ describes a small deviation from a homogeneous and isotropic universe, c_e is the effective sound speed of dark energy which is set to 1 in this work, c_a is the adiabatic sound speed of dark energy, and \mathcal{R} is the energy density ratio of dark matter to dark energy, i.e., $\mathcal{R} = \rho_c/\rho_d$.

III. THE KIDS AND PLANCK DATASETS

The KiDS is optimally designed to measure shapes of galaxies with photometric redshifts so a study of weak lensing tomography can be performed. In this work we use angular correlation functions measured from KiDS's 450 degree square data to constrain our IDMDE models.

The angular shear correlation function ξ_{\pm}^{ij} between redshifts i and j is given by the convergence power spectrum via

$$\xi_{\pm}^{ij}(\theta) = \frac{1}{2\pi} \int d\ell \ell P_{\kappa}^{ij} J_{0,4}(\ell\theta), \quad (7)$$

where θ is the angular position on the sky, ℓ is the angular wave number, and $J_{0,4}(\ell\theta)$ are the zeroth and the fourth order Bessel functions of the first kind for ξ_+ and ξ_- , respectively. According to the Limber approximation,

the convergence power spectrum P_{κ}^{ij} can be written as

$$P_{\kappa}^{ij} = \int_0^{\chi_H} d\chi \frac{W_i(\chi)W_j(\chi)}{\chi^2} P_{\delta} \left(\frac{l}{\chi}, \chi \right), \quad (8)$$

where χ is comoving distance, χ_H is the comoving distance evaluated at an infinite redshift, $W_i(\chi)$ is the lensing weighting function corresponding to a redshift bin i , and P_{δ} is a non-linear matter power spectrum derived from a IDMDE model. The lensing weighting function $W_i(\chi)$ is [1]

$$W_i(\chi) = \frac{3H_0^2\Omega_{m0}}{2c^2a(\chi)} \chi \int_{\chi}^{\chi_H} d\chi' n_i(\chi') \frac{\chi' - \chi}{\chi'}, \quad (9)$$

for the standard Λ CDM model. But this expression is not valid when there is interaction between dark sectors, since the relation of the standard dark matter density evolution $\Omega_c/\Omega_{c0} = H_0^2/(a^3H^2)$ fails for interacting dark energy models. Instead, equation (9) should be written in the general form [34]

$$W_i(\chi) = \frac{3a(\chi)^2H(\chi)^2\Omega_m(\chi)}{2c^2} \chi \int_{\chi}^{\chi_H} d\chi' n_i(\chi') \frac{\chi' - \chi}{\chi'}, \quad (10)$$

where $\Omega_m = \rho_m/\rho_{\text{crit}}$, the critical density $\rho_{\text{crit}} = 3H^2/(8\pi G)$, c is the speed of light, n_i is the galaxy redshift distribution in the bin i and it is normalized as $\int_0^{\chi_H} n(\chi) d\chi = 1$.

The KiDS-450 datasets consist of four tomographic redshift bins ($0.1 < z < 0.3$, $0.3 < z < 0.5$, $0.5 < z < 0.7$, $0.7 < z < 0.9$), and nine angular bins centered at $\theta = (0.7134', 1.452', 2.956', 6.017', 12.25', 24.93', 50.75', 103.3', 210.3')$. For each tomographic redshift pair (ij), the angular ranges are limited to $\theta < 72'$ for ξ_+^{ij} and $\theta > 4.2'$ for ξ_-^{ij} , so the last two bins and first three bins for ξ_+^{ij} and ξ_-^{ij} are masked out, respectively. Eventually there are 130 angular band powers in this datasets which can be used to constrain the IDMDE models [7].

In addition to the KiDS-450 datasets, we also use the latest CMB power spectra from Planck 2015 data release [35] to derive constraints, which can be directly compared to the previous ones, for our IDMDE models [33, 36]. Similar to [36], we take all the CMB temperature and polarization power spectra within $2 < \ell < 2000$ except the BB power spectrum for which only the low- ℓ , i.e. $2 < \ell < 30$, measurement is made available.

To sample parameter space of our cosmological models, we carry out a series of Markov Chain Monte Carlo (MCMC) runs using the modified CosmoMC code package [1] that has already integrated the weak lensing module as described in [7]. We assume a flat universe with no running of the spectral index. We fix the effective number of neutrino species to $N_{\text{eff}} = 3.046$, the sum of

neutrino masses to $\Sigma m_{\nu} = 0.06$ eV, and the primordial helium fraction $Y_p = 0.25$. For the MCMC runs, a convergence criterion is set to $R - 1 = 0.02$ where R is the Gelman–Rubin threshold [37].

Before we launch the MCMC runs, priors on cosmological parameters are chosen and listed in Table II. These priors are chosen the same as the ones in [36] because we want to validate that our analysis with the same model, so that comparisons can be carried out by constraining the IDMDE models using the Planck data available in [36] and the weak lensing data, and examining the concordance problem with these two different datasets.

TABLE II: Priors on cosmological parameters for phenomenological IDMDE models

Parameter	Prior			
$\Omega_b h^2$	[0.005, 0.1]			
$\Omega_c h^2$	[0.001, 0.99]			
100θ	[0.5, 10]			
τ	[0.01, 0.8]			
n_s	[0.9, 1.1]			
$\log(10^{10} A_s)$	[2.7, 4]			
h	[0.4, 1]			
Model	I	II	III	IV
w	[-1, -0.3]	[-3, -1]	[-3, -1]	[-3, -1]
λ_i	[-0.4, 0]	[0, 0.4]	[0.0, 0.1]	[0, 0.01]

IV. RESULTS

Before investigating the IDMDE models, we first compare the theoretical predictions of the weak lensing correlation functions from the standard Λ CDM model to both KiDS and Planck measurements. In Fig. 1 we show parameter constraints for KiDS in the σ_8 – Ω_m plane using priors in Table II, where the amplitude of scalar perturbation A_s and the scalar spectral index n_s are limited to much narrower parameter space, as compared to those in [7]. These priors shrink the parameter contours and thereby increase the tension between KiDS weak lensing and Planck CMB temperature measurements for the Λ CDM model as Fig. 1 clearly shows. The main reason for choosing the same priors in Table II, as Table 3 in [36] instead of those exactly from [7], is to compare our model fitting to KiDS datasets with that to Planck datasets which was already available in [36], especially in the following discussions for the IDMDE models.

In this section, we will investigate the IDMDE models and examine how these models are favored by both datasets and to what extent they will alleviate the tension.

[1] <https://github.com/sjoudaki/kids450>

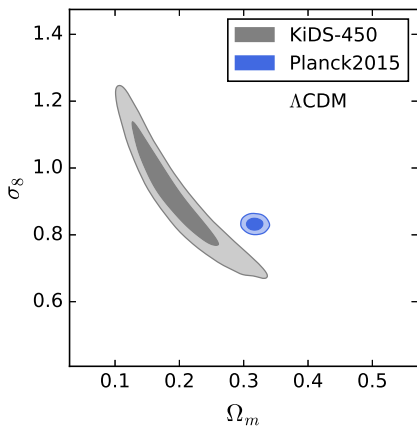


FIG. 1: Marginalized posterior distribution function in the $\sigma_8 - \Omega_m$ plane for the Λ CDM model. 68% and 95% confidence levels are shown as inner and outer regions.

A. Model selection

We now use the IDMDE models to predict the CMB power spectra and weak lensing shear correlation functions and compare them to the Planck and the KiDS-450 datasets, and the two sets of constraints that are derived from the IDMDE and the standard Λ CDM models will be passed along the Deviance Information Criterion (DIC) [12, 38] to determine which model is more favored. The DIC is composed of the sum of goodness of fit of a given model and its Bayesian complexity, and it is defined as

$$\text{DIC} = \chi_{\text{eff}}^2(\hat{\theta}) + 2p_{\text{D}}, \quad (11)$$

where $\chi_{\text{eff}}^2(\hat{\theta}) = -2\ln\mathcal{L}_{\text{max}}$ is the best-fit effective χ^2 and $\hat{\theta}$ is the parameter vector at the maximum likelihood point. The generic form of χ^2 is expressed as $\Delta\xi^T \mathbf{Cov}^{-1} \Delta\xi$, where $\Delta\xi = \xi_{\text{obs}} - \xi_{\text{theory}}$, ξ_{obs} is a 130-element vector of the measured weak lensing correlation functions from the KiDS project, ξ_{theory} is the theoretical prediction from equation (7), and \mathbf{Cov} , which is a 130×130 covariance matrix at each angular scale, is also provided by the KiDS data release.

The second term in equation (11) is the Bayesian complexity expressed as $p_{\text{D}} = \langle \chi_{\text{eff}}^2(\theta) \rangle - \chi_{\text{eff}}^2(\hat{\theta})$, where $\langle \chi_{\text{eff}}^2(\theta) \rangle$ represents the mean χ^2 averaged over the posterior distribution. We define the differences in DIC as

$$\Delta\text{DIC} = \text{DIC}(\text{IDMDE}) - \text{DIC}(\Lambda\text{CDM}), \quad (12)$$

and the condition of $\Delta\text{DIC} < -5$ indicates a moderate preference in favor of the IDMDE model while the condition $\Delta\text{DIC} \sim 0$ means that one model is not favored over the other [7].

In Table III, we calculate changes relative to the reference Λ CDM model in both $\chi_{\text{eff}}^2(\hat{\theta})$ and DIC for four IDMDE models, where the negative values of DIC indicate preference in favor of the IDMDE models. In all of

the IDMDE models, we find that either KiDS or Planck on its own does not show any preference for the IDMDE models because $|\Delta\text{DIC}|$ is always smaller than 5. But the combination of KiDS and Planck datasets does favor the IDMDE models with strong negative ΔDIC values.

TABLE III: $\Delta\chi_{\text{eff}}^2(\hat{\theta})$ and ΔDIC between the IDMDE models and the reference Λ CDM model. $\Delta\chi_{\text{eff}}^2$ is the minimum χ^2 difference between the model and Λ CDM.

Model	Data	$\Delta\chi_{\text{eff}}^2$	ΔDIC
I	KiDS	2.016	6.02
	Planck	1.368	3.856
	KiDS+Planck	-19.094	-24.299
II	KiDS	-0.813	0.578
	Planck	-2.676	-1.735
	KiDS+Planck	-5.762	-9.380
III	KiDS	-1.174	0.480
	Planck	-1.292	-0.611
	KiDS+Planck	-5.460	-10.808
IV	KiDS	-0.710	0.511
	Planck	-1.550	-0.816
	KiDS+Planck	-3.986	-12.385

In Fig. (3), we show the parameter constraints in the $\sigma_8 - \Omega_m$ plane for all of the IDMDE models. The KiDS constraints are in gray and the Planck constraints are in blue. Different from the constraints of the Λ CDM model in Fig. (1), Fig. (3) shows that the KiDS and Planck constraints of the IDMDE models start to overlap with each other.

In order to quantify at what level the tension between KiDS and Planck has been reduced by the IDMDE models, a tension parameter T is adopted and it is defined as [7]

$$T(S_8) = \frac{|\langle S_8^K \rangle - \langle S_8^P \rangle|}{\sqrt{\sigma^2(S_8^K) + \sigma^2(S_8^P)}}. \quad (13)$$

Here $S_8 = \sigma_8 \sqrt{\Omega_m}$, $\langle S_8 \rangle$ is the mean value over the posterior distribution, σ is the standard deviation, and the superscripts K and P correspond to KiDS and Planck, respectively.

In Table IV, we list all the values of $T(S_8)$ for Λ CDM and the IDMDE models. It is quite obvious that the IDMDE models can reduce discordance significance to $\sim 1\sigma$ level, substantially relieving the 2σ -level tension inferred from the standard Λ CDM model. Among all the IDMDE models, the T -parameter values can further indicate that Model I has the least discordance between two datasets while other IDMDE models have roughly the same level of discordance. The overlapped contours are shown in Fig. (3).

In Model I, the blue contours from Planck show significantly different directions compared to that in the Λ CDM model because the posterior distribution functions are

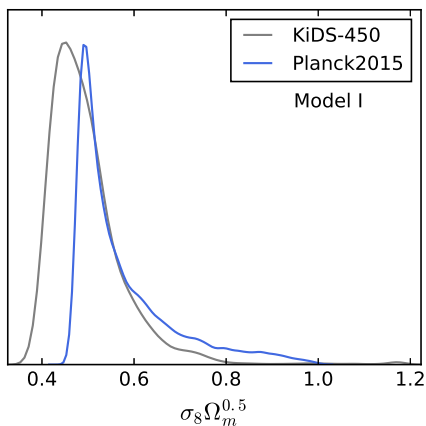


FIG. 2: 1D distributions of S_8 for KiDS and Planck.

considerably skewed compared with other IDMDE models. And this is verified in Fig. (2), where probability distribution of the parameter S_8 is not symmetric. So we should note that the T -parameter defined in Eq. (13) may not be a very appropriate method for quantifying the discordance of Model I.

From both the DIC and the T -parameter tests, we find that the IDMDE models can effectively alleviate the tensions between KiDS and Planck datasets, thereby they are more favored than the Λ CDM model by the data.

TABLE IV: The values of $T(S_8)$ for the Λ CDM and four interacting dark energy models shown in Table I.

Model	Λ CDM	I	II	III	IV
$T(S_8)$	2.11σ	0.44σ	1.08σ	1.18σ	1.24σ

B. Model constraints

In this section, we present all the results from the MCMC runs. We derive constraints for the IDMDE models from the KiDS-450 datasets and compare them to the previous limits set by Planck data [36]. We perform the joint analysis with both the KiDS and Planck data and list all the best-fit values and 68% confidence regions in Tables V, VI, VII and VIII. The 1D marginalized posterior distribution functions (PDFs) are shown for the parameters $\Omega_c h^2$, w , λ_i , and H_0 in Fig. (4) and the 2D functions in Fig. (5).

(1) Model I: the 1D PDFs are shown for the parameters $\Omega_c h^2$, w , λ_2 , and H_0 in Fig. (4a) and the 2D PDFs in Fig. (5a). Due to large band power uncertainties, we find that the constraints from the KiDS data alone have wider 1σ and 2σ contours compared to Planck for most of the parameters. However, we find that the 68% confidence regions of $\Omega_c h^2$, λ_2 , Ω_d and Ω_m from KiDS data (in Table V) are smaller than constraints from the Planck data

and this indicates that the weak lensing measurements are more sensitive to the interaction and the energy densities of dark sectors compared to the cosmic microwave background measurements. Among all the constraints from both the KiDS and Planck datasets, Model I is of particular interest in that KiDS data alone can give a negative coupling parameter λ_2 , which is in agreement with the Planck constraint [36], and the sign of the coupling does not change even if the KiDS and Planck datasets are combined. The negative coupling indicates that the energy flows from dark matter to dark energy, unfortunately, the IDMDE models with negative couplings are not favored to alleviate the coincidence problem, see review and references therein for detailed explanations [30]. Therefore, Model I can achieve a concordance between observational datasets at the cost of intensifying the coincidence problem.

(2) Models II, III and IV: the 1D and 2D marginalized PDFs are shown in Figs. (4b, 4c, 4d) and Figs. (5b, 5c, 5d), respectively. Similar to Model I, the Planck measurements always have tighter constraints on most of the parameters as compared to the KiDS measurements. The positive sign of the constrained parameter λ_2 indicates that there is energy transferred from dark energy to dark matter so the duration for the energy densities of dark matter and dark energy being comparable is much longer than Λ CDM, alleviating the coincidence problem [33].

The KiDS-only constraint on σ_8 for the standard model is $\sigma_8 = 0.849^{+0.120}_{-0.204}$ [1], and its constraint on H_0 of the standard model is also found reasonable therein. Now with the extra degree of freedom introduced in the IDMDE models, Table V shows that the KiDS-only constraint on σ_8 in Model I is quite large, inconsistent with other cosmological observations, and so are the values of the Hubble constant H_0 that are shown in Tables VI, VII and VIII, corresponding to the three IDMDE models. Despite high values, these results are still consistent with the previous Planck-only constraints [36]. Also, these high values, which could be considered as unreasonable constraints, can be easily reduced by adding more observational datasets such as BAO and SNIa, as done in [36]. Similarly, the high values derived from the KiDS-only measurements could be reduced as well, by adding those observations. However, in the scope of this work, we exclusively focus on the discordance problem found in the standard Λ CDM model between weak lensing and Planck datasets, not the most stringent limits from multiple observational datasets. Specifically, our motivation is to investigate if the discordance can be alleviated by the IDMDE models. From the analysis in this work, it is proven that the tension between Planck and KiDS datasets is indeed alleviated.

V. CONCLUSIONS

In this work we have obtained the observational constraints on the IDMDE models using both weak gravi-

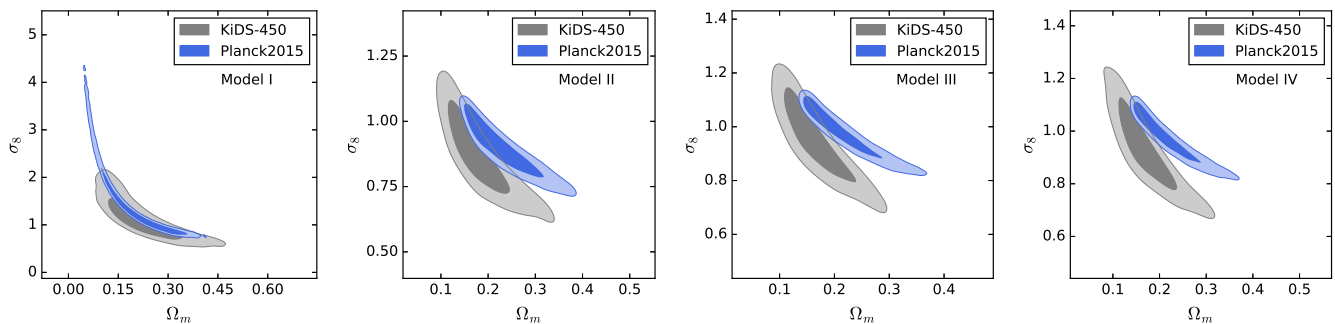


FIG. 3: Marginalized confidence contours in the $\sigma_8 - \Omega_m$ plane for four IDMDE models. 68% and 95% confidence levels are shown as inner and outer regions.

tational lensing data from the KiDS and the CMB data from Planck. We have examined how the IDMDE models are favored by data as compared to the standard Λ CDM and to what extent the IDMDE models can relieve the tensions between KiDS and Planck CMB datasets. Employing the DIC and T -parameter diagnostics, we find with great interest that a desired concordance between KiDS and Planck datasets can be achieved by the IDMDE models which are more preferred than the standard Λ CDM model.

We obtain parameter constraints on the IDMDE models from KiDS measurements, Planck measurements and the combination. Due to large band-power uncertainties in the weak lensing measurements, the KiDS data alone always have less constraining power than the Planck datasets for most of the parameters but a joint fit to both datasets can always improve the constraints significantly.

For model I, the sign of the interaction parameter being negative indicates that the energy flows from dark matter to dark energy. And this scenario is not favored to the alleviation of the coincidence problem. While the other three models favor a scenario with energy flowing from dark energy to dark matter, which thus can alleviate the coincidence problem.

Acknowledgments

We thank Jun Zhang and Zuhui Fan for helpful comments and suggestions. This work was partially supported by National Basic Research Program of China (973 Program 2013CB834900) and National Natural Science Foundation of China.

-
- [1] Hildebrandt H., Viola M., Heymans C., et al, “KiDS-450: cosmological parameter constraints from tomographic weak gravitational lensing”, *Monthly Notices of the Royal Astronomical Society*, 465 (2017) 1454, [[arXiv:1606.05338](#)].
- [2] de Jong J. T. A., Verdoes Kleijn G. A., Boxhoorn D. R., et al, “The first and second data releases of the Kilo-Degree Survey”, *Astronomy & Astrophysics*, 582 (2015) A62, [[arXiv:1507.00742](#)].
- [3] Kuijken K., Heymans C., Hildebrandt H., et al, “Gravitational lensing analysis of the Kilo-Degree Survey”, *Monthly Notices of the Royal Astronomical Society*, 454 (2015) 3500, [[arXiv:1507.00738](#)].
- [4] Fenech Conti I., Herbonnet R., Hoekstra H., et al, “Calibration of weak-lensing shear in the Kilo-Degree Survey”, *Monthly Notices of the Royal Astronomical Society*, 467 (2017) 1627, [[arXiv:1606.05337](#)].
- [5] Planck Collaboration, Ade P. A. R., Aghanim N., et al., “Planck 2015 results. XIII. Cosmological parameters”, *Astronomy & Astrophysics*, 594 (2016) A13, [[arXiv:1502.01589](#)].
- [6] Planck Collaboration, Aghanim N., Arnaud M., et al., “Planck 2015 results. XI. CMB power spectra, likelihoods, and robustness of parameters”, *Astronomy & Astrophysics*, 594 (2016) A11, [[arXiv:1507.02704](#)].
- [7] Joudaki S., Mead A., Blake C., et al, “KiDS-450: testing extensions to the standard cosmological model”, *Monthly Notices of the Royal Astronomical Society*, 471 (2017) 1259, [[arXiv:1610.04606](#)].
- [8] Heymans C., Van Waerbeke L., Miller L., et al., “CFHTLenS: the Canada-France-Hawaii Telescope Lensing Survey”, *Monthly Notices of the Royal Astronomical Society*, 427 (2012) 146, [[arXiv:1210.0032](#)].
- [9] Hildebrandt H., Erben T., Kuijken K., et al., “CFHTLenS: improving the quality of photometric redshifts with precision photometry”, *Monthly Notices of the Royal Astronomical Society*, 421 (2012) 2355, [[arXiv:1111.4434](#)].
- [10] Erben T., Hildebrandt H., Miller L., et al., “CFHTLenS: the Canada-France-Hawaii Telescope Lensing Survey - imaging data and catalogue products”, *Monthly Notices of the Royal Astronomical Society*, 433 (2013) 2545, [[arXiv:1210.8156](#)].
- [11] Miller L., Heymans C., Kitching T. D., et al., “Bayesian galaxy shape measurement for weak lensing surveys - III. Application to the Canada-France-Hawaii Telescope Lensing Survey”, *Monthly Notices of the Royal Astronomical Society*, 429 (2013) 2858, [[arXiv:1210.8201](#)].

- [12] Joudaki S., Blake C., Heymans C., et al., “CFHTLenS revisited: assessing concordance with Planck including astrophysical systematics”, *Monthly Notices of the Royal Astronomical Society*, 465, (2017) 2033, [arXiv:1601.05786].
- [13] Planck Collaboration, Ade P. A. R., Aghanim N., et al., “Planck 2013 results. XVI. Cosmological parameters”, *Astronomy & Astrophysics*, 571 (2014) A16, [arXiv:1303.5076].
- [14] MacCrann, N., Zuntz, J., Bridle, S., Jain, B., “Cosmic discordance: are Planck CMB and CFHTLenS weak lensing measurements out of tune?”, *Monthly Notices of the Royal Astronomical Society*, 451 (2015) 2877, [arXiv:1408.4742].
- [15] Köhlinger F., Viola M., Valkenburg W., et al., “A direct measurement of tomographic lensing power spectra from CFHTLenS”, *Monthly Notices of the Royal Astronomical Society*, 456 (2016) 1508, [arXiv:1509.04071].
- [16] Riess A. G., Macri L., Casertano S., et al., “A 3% Solution: Determination of the Hubble Constant with the Hubble Space Telescope and Wide Field Camera 3”, *The Astrophysical Journal*, 730 (2011) 119, [arXiv:1103.2976].
- [17] Riess A. G., Macri L. M., Hoffmann S. L., et al., “A 2.4% Determination of the Local Value of the Hubble Constant”, *The Astrophysical Journal*, 826 (2016) 56, [arXiv:1604.01424].
- [18] Delubac T., Bautista J. E., Busca N. G., et al., “Baryon acoustic oscillations in the Ly α forest of BOSS DR11 quasars”, *Astronomy & Astrophysics*, 574 (2015) A59, [arXiv:1404.1801].
- [19] Kunz M., Nesseris S., & Sawicki I., “Using dark energy to suppress power at small scales”, *Physical Review D*, 92 (2015) 063006, [arXiv:1507.01486].
- [20] Bernal J. L., Verde L., & Riess A. G., “The trouble with H_0 ”, *Journal of Cosmology and Astroparticle Physics*, 10 (2016) 019, [arXiv:1607.05617].
- [21] Di Valentino E., Melchiorri A., & Silk J., “Reconciling Planck with the local value of H_0 in extended parameter space”, *Physics Letters B*, 761 (2016) 242, [arXiv:1606.00634].
- [22] Ferreira E. G. M., Quintin J., Costa A. A., Abdalla E., & Wang B., “Evidence for interacting dark energy from BOSS”, *Physical Review D*, 95 (2017) 043520, [arXiv:1412.2777].
- [23] Weinberg S., “The cosmological constant problem”, *Reviews of Modern Physics*, 61 (1989) 1.
- [24] Chimento L. P., Jakubi A. S., Pavón D., & Zimdahl W., “Interacting quintessence solution to the coincidence problem”, *Physical Review D*, 67 (2003) 083513, [arXiv:astro-ph/0303145].
- [25] Amendola L., “Coupled quintessence”, *Physical Review D*, 62 (2000) 043511, [arXiv:astro-ph/9908023]; Amendola L., & Quercellini C., “Tracking and coupled dark energy as seen by the Wilkinson Microwave Anisotropy Probe”, *Physical Review D*, 68 (2003) 023514, [arXiv:astro-ph/0303228]; Amendola L., Tsujikawa S., & Sami M., “”, *Physics Letters B*, 632 (2006) 155, [arXiv:astro-ph/0506222].
- [26] Pavón D., & Zimdahl W., “Holographic dark energy and cosmic coincidence”, *Physics Letters B*, 628 (2005) 206, [arXiv:gr-qc/0505020]; Del Campo, S., Herrera R., & Pavón D., “Toward a solution of the coincidence problem”, *Physical Review D*, 78 (2008) 021302, [arXiv:0806.2116].
- [27] Böhmer C. G., Caldera Cabral G., Lazkoz R., & Maartens R., “Dynamics of dark energy with a coupling to dark matter”, *Physical Review D*, 78 (2008) 023505, [arXiv:0801.1565].
- [28] Olivares G., Atrio Barandela F., & Pavón D., “Matter density perturbations in interacting quintessence models”, *Physical Review D*, 74 (2006) 043521, [arXiv:astro-ph/0607604].
- [29] Chen S., Wang B., & Jing J., “Dynamics of an interacting dark energy model in Einstein and loop quantum cosmology”, *Physical Review D*, 78 (2008) 123503, [arXiv:0808.3482].
- [30] Wang B., Abdalla E., Atrio Barandela F., & Pavón D., “Dark matter and dark energy interactions: theoretical challenges, cosmological implications and observational signatures”, *Reports on Progress in Physics*, 79 (2016) 096901, [arXiv:1603.08299].
- [31] He J.-H., Wang B., & Abdalla E., “Stability of the curvature perturbation in dark sectors’ mutual interacting models”, *Physics Letters B*, 671 (2009) 139, [arXiv:0807.3471].
- [32] Gavela M. B., Hernández D., Lopez Honorez L., Mena O., & Rigolin S., “Dark coupling”, *Journal of Cosmology and Astroparticle Physics*, 7 (2009) 034, [arXiv:0901.1611].
- [33] Costa A. A., Xu X.-D., Wang B., Ferreira E. G. M., & Abdalla E., “Testing the interaction between dark energy and dark matter with Planck data”, *Physical Review D*, 89 (2013) 103531, [arXiv:1311.7380].
- [34] Schaefer B. M., Caldera Cabral G. A., & Maartens R., “Constraints on the decay of dark matter to dark energy from weak lensing bispectrum tomography”, [arXiv:0803.2154].
- [35] Planck Collaboration, Adam R., Ade P. A. R., et al., “Planck 2015 results. I. Overview of products and scientific results”, *Astronomy & Astrophysics*, 594 (2016) A1, [arXiv:1502.01582].
- [36] Costa A. A., Xu X.-D., Wang B., & Abdalla E., “Constraints on interacting dark energy models from Planck 2015 and redshift-space distortion data”, *Journal of Cosmology and Astroparticle Physics*, 1 (2017) 028, [arXiv:1605.04138].
- [37] Andrew G. & Donald B. R., “Inference from Iterative Simulation Using Multiple Sequences”, *Statistical Science*, 7 (1992) 457-472.
- [38] Spiegelhalter D. J., Best N. G., Carlin B. P., Van Der Linde A., “Bayesian measures of model complexity and fit”, *Journal of the Royal Statistical Society: Series B (Statistical Methodology)*, 64 (2002) 583.

TABLE V: Best fit values and 68% confidence levels for parameters in Model I.

Parameter	KiDS		Planck		KiDS+Planck	
	Best fit	68% limits	Best fit	68% limits	Best fit	68% limits
$\Omega_b h^2$	0.01380	$0.04324^{+0.01186}_{-0.03824}$	0.02231	$0.0222^{+0.00016}_{-0.00016}$	0.02119	$0.02121^{+0.000152}_{-0.000174}$
$\Omega_c h^2$	0.09104	$0.08022^{+0.02162}_{-0.04046}$	0.04788	$0.07131^{+0.0472}_{-0.024}$	0.06127	$0.06287^{+0.00744}_{-0.01427}$
100θ	1.108	$1.033^{+0.05013}_{-0.06933}$	1.045	$1.044^{+0.0015}_{-0.00329}$	1.044	$1.044^{+0.001104}_{-0.000665}$
τ	0.4419	$0.4122^{+0.1533}_{-0.4022}$	0.08204	$0.08063^{+0.0171}_{-0.0169}$	0.04309	$0.04377^{+0.0164}_{-0.02402}$
$\ln(10^{10} A_s)$	3.636	$3.249^{+0.1710}_{-0.5494}$	3.102	$3.097^{+0.0328}_{-0.0329}$	3.020	$3.021^{+0.0349}_{-0.0472}$
n_s	0.9435	$0.9931^{+0.1068}_{-0.09315}$	0.9639	$0.9633^{+0.00472}_{-0.00514}$	0.9453	$0.9495^{+0.00465}_{-0.00511}$
w	-0.8682	$-0.7811^{+0.05257}_{-0.2178}$	-0.9765	$-0.9031^{+0.023}_{-0.0959}$	-0.9554	$-0.9079^{+0.0217}_{-0.082}$
λ_2	-0.01512	> -0.1237	-0.1831	> -0.1745	-0.1871	$-0.1780^{+0.0215}_{-0.0456}$
H_0	84.35	$76.10^{+17.62}_{-11.95}$	72.36	$68.1^{+2.99}_{-3.2}$	68.46	$67.27^{+2.44}_{-1.16}$
Ω_d	0.8517	$0.7792^{+0.09475}_{-0.05074}$	0.8647	$0.7899^{+0.0932}_{-0.106}$	0.8227	$0.8119^{+0.0484}_{-0.0163}$
Ω_m	0.1482	$0.2207^{+0.05074}_{-0.09475}$	0.1353	$0.2101^{+0.106}_{-0.0926}$	0.1773	$0.1881^{+0.0163}_{-0.0484}$
σ_8	1.107	$1.131^{+0.1883}_{-0.3978}$	1.622	$1.438^{+0.143}_{-0.789}$	1.385	$1.359^{+0.235}_{-0.191}$
Age/Gyr	12.74	$12.52^{+1.531}_{-2.311}$	13.71	$13.81^{+0.058}_{-0.0916}$	13.86	$13.91^{+0.0288}_{-0.0496}$

TABLE VI: Best fit values and 68% confidence levels for parameters in Model II.

Parameter	KiDS		Planck		KiDS+Planck	
	Best fit	68% limits	Best fit	68% limits	Best fit	68% limits
$\Omega_b h^2$	0.01020	$0.02355^{+0.003478}_{-0.01855}$	0.02232	$0.02225^{+0.000162}_{-0.000161}$	0.02137	$0.02149^{+0.000122}_{-0.000141}$
$\Omega_c h^2$	0.1063	$0.1176^{+0.02170}_{-0.02790}$	0.1314	$0.1334^{+0.00692}_{-0.0125}$	0.12033	$0.12136^{+0.00134}_{-0.00226}$
100θ	1.061	$1.034^{+0.05504}_{-0.05481}$	1.04	$1.04^{+0.000651}_{-0.000562}$	1.040	$1.040^{+0.000321}_{-0.000309}$
τ	0.2427	$0.4004^{+0.3974}_{-0.3876}$	0.07543	$0.07653^{+0.0177}_{-0.0174}$	0.01224	$0.02201^{+0.00306}_{-0.01201}$
$\ln(10^{10} A_s)$	3.466	$3.151^{+0.1323}_{-0.4516}$	3.082	$3.088^{+0.0342}_{-0.0337}$	2.951	$2.967^{+0.0109}_{-0.0245}$
n_s	1.039	$1.015^{+0.08414}_{-0.02851}$	0.9657	$0.9638^{+0.00477}_{-0.00475}$	0.9547	$0.9575^{+0.00406}_{-0.00408}$
w	-1.370	$-1.397^{+0.06139}_{-0.06139}$	-1.872	$-1.55^{+0.235}_{-0.358}$	-1.977	$-1.780^{+0.089}_{-0.215}$
λ_2	0.02176	< 0.00294	0.02931	< 0.05044	0.00008	< 0.00564
H_0	99.52	$88.13^{+11.64}_{-3.988}$	96.2	$83.88^{+13.3}_{-7.86}$	98.3	$92.04^{+7.81}_{-2.36}$
Ω_d	0.8816	$0.8135^{+0.06042}_{-0.03261}$	0.8331	$0.7688^{+0.0778}_{-0.0353}$	0.8527	$0.828^{+0.0305}_{-0.0067}$
Ω_m	0.1183	$0.1864^{+0.03261}_{-0.06042}$	0.1669	$0.2312^{+0.0353}_{-0.0778}$	0.1473	$0.172^{+0.0067}_{-0.0305}$
σ_8	1.046	$0.8548^{+0.1091}_{-0.1311}$	0.9852	$0.9016^{+0.0945}_{-0.094}$	1.0283	$0.9725^{+0.061}_{-0.0382}$
Age/Gyr	13.62	$13.58^{+1.181}_{-1.845}$	13.46	$13.59^{+0.0708}_{-0.143}$	13.55	$13.38^{+0.028}_{-0.064}$

TABLE VII: Best fit values and 68% confidence levels for parameters in Model III.

Parameter	KiDS		Planck		KiDS+Planck	
	Best fit	68% limits	Best fit	68% limits	Best fit	68% limits
$\Omega_b h^2$	0.006800	$0.02134^{+0.002548}_{-0.01634}$	0.0223	$0.02235^{+0.00017}_{-0.00017}$	0.0214	$0.02148^{+0.000133}_{-0.000137}$
$\Omega_c h^2$	0.1007	$0.1078^{+0.01939}_{-0.02530}$	0.1198	$0.1236^{+0.00235}_{-0.00353}$	0.1207	$0.0120^{+0.0012}_{-0.00114}$
100θ	1.094	$1.050^{+0.05750}_{-0.05642}$	1.041	$1.041^{+0.000377}_{-0.000374}$	1.041	$1.040^{+0.000306}_{-0.000306}$
τ	0.03344	$0.4049^{+0.3950}_{-0.3949}$	0.07784	$0.07051^{+0.0182}_{-0.0179}$	0.0149	$0.0218^{+0.0021}_{-0.011}$
$\ln(10^{10} A_s)$	3.565	$3.283^{+0.1875}_{-0.5839}$	3.087	$3.074^{+0.0357}_{-0.0355}$	2.956	$2.966^{+0.0103}_{-0.0233}$
n_s	0.9392	$1.018^{+0.08126}_{-0.02662}$	0.9649	$0.9608^{+0.00508}_{-0.00503}$	0.9571	$0.9568^{+0.004}_{-0.00406}$
w	-1.228	$-1.393^{+0.3929}_{-0.07466}$	-1.701	$-1.702^{+0.298}_{-0.364}$	-1.98	$-1.807^{+0.0765}_{-0.223}$
λ_1	0.002013	< 0.006058	0.0004372	< 0.001831	0.00005	< 0.00013
H_0	99.28	$88.71^{+11.16}_{-3.237}$	89.51	$84.91^{+15.1}_{-4.8}$	98.1	$92.45^{+6.55}_{-1.9}$
Ω_d	0.8902	$0.8308^{+0.05582}_{-0.02877}$	0.8218	$0.788^{+0.0686}_{-0.0268}$	0.8516	$0.8308^{+0.0275}_{-0.0044}$
Ω_m	0.1098	$0.1691^{+0.02877}_{-0.05582}$	0.1782	$0.212^{+0.0268}_{-0.0686}$	0.1484	$0.1692^{+0.0044}_{-0.0275}$
σ_8	1.201	$0.9538^{+0.1272}_{-0.1274}$	1.016	$0.9885^{+0.102}_{-0.061}$	1.034	$0.9905^{+0.0593}_{-0.0211}$
Age/Gyr	1.312	$13.64^{+1.177}_{-1.823}$	13.55	$13.71^{+0.102}_{-0.18}$	13.55	$13.60^{+0.0941}_{-0.065}$

TABLE VIII: Best fit values and 68% confidence levels for parameters in Model IV.

Parameter	KiDS		Planck		KiDS+Planck	
	Best fit	68% limits	Best fit	68% limits	Best fit	68% limits
$\Omega_b h^2$	0.009471	$0.02191^{+0.002329}_{-0.01691}$	0.0223	$0.02235^{+0.000178}_{-0.000179}$	0.0214	$0.02148^{+0.00023}_{-0.00014}$
$\Omega_c h^2$	0.1077	$0.1108^{+0.02003}_{-0.02752}$	0.1209	$0.124^{+0.0025}_{-0.0039}$	0.1206	$0.120^{+0.0011}_{-0.0012}$
100θ	1.136	$1.048^{+0.06034}_{-0.06127}$	1.041	$1.041^{+0.000375}_{-0.000373}$	1.041	$1.040^{+0.00029}_{-0.00028}$
τ	0.4306	$0.3863^{+0.4136}_{-0.3763}$	0.084	$0.07043^{+0.018}_{-0.0176}$	0.0128	$0.02146^{+0.00268}_{-0.01246}$
$\ln(10^{10} A_s)$	3.644	$3.2435^{+0.1714}_{-0.5435}$	3.1	$3.073^{+0.0351}_{-0.0344}$	2.953	$2.966^{+0.01068}_{-0.01722}$
n_s	0.9346	$1.017^{+0.08255}_{-0.02786}$	0.9634	$0.9609^{+0.00512}_{-0.00518}$	0.9565	$0.9567^{+0.00404}_{-0.004}$
w	-1.024	$-1.459^{+0.4580}_{-0.08525}$	-1.674	$-1.691^{+0.318}_{-0.359}$	-2.012	$-1.828^{+0.078}_{-0.184}$
λ	0.0006674	< 0.005621	0.0007646	< 0.001781	0.00022	< 0.00013
H_0	99.04	$89.28^{+10.65}_{-3.448}$	87.25	$84.63^{+15.4}_{-4.9}$	98.95	$93.2^{+6.67}_{-2.203}$
Ω_d	0.8798	$0.8300^{+0.05207}_{-0.02780}$	0.8111	$0.7859^{+0.07}_{-0.0275}$	0.8543	$0.834^{+0.024}_{-0.006}$
Ω_m	0.1201	$0.1699^{+0.02780}_{-0.05207}$	0.1889	$0.2141^{+0.0275}_{-0.07}$	0.1457	$0.166^{+0.006}_{-0.024}$
σ_8	1.203	$0.9302^{+0.1089}_{-0.1083}$	1.006	$0.9833^{+0.102}_{-0.0636}$	1.034	$0.9958^{+0.05}_{-0.0217}$
Age/Gyr	12.17	$13.67^{+1.259}_{-2.018}$	13.61	$13.71^{+0.102}_{-0.176}$	13.56	$13.59^{+0.0291}_{-0.0557}$

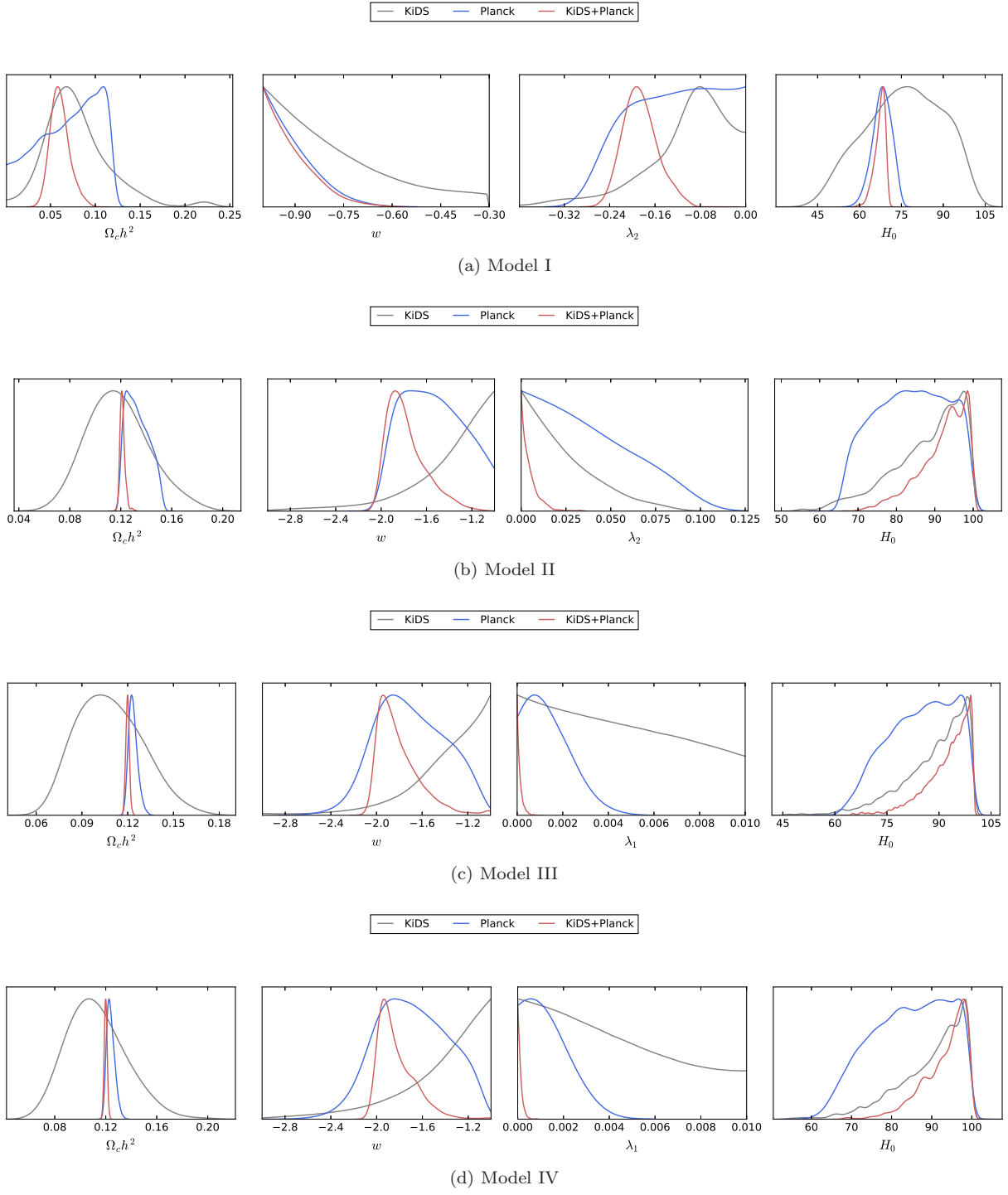
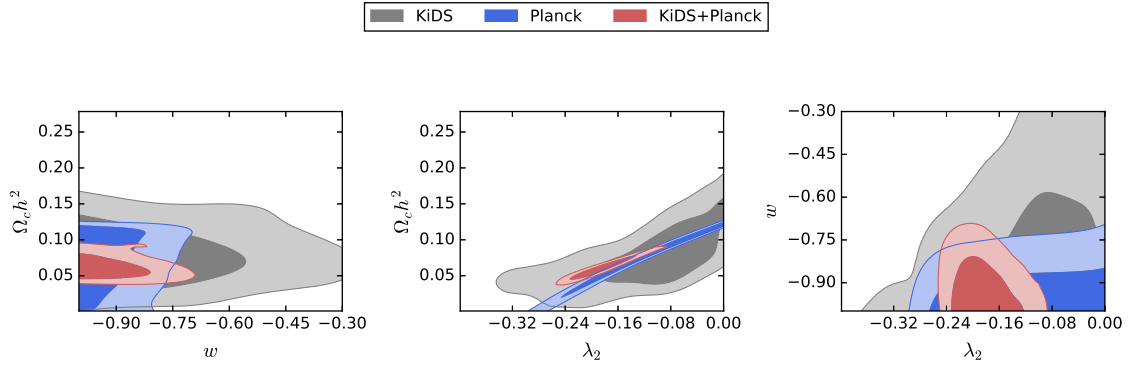
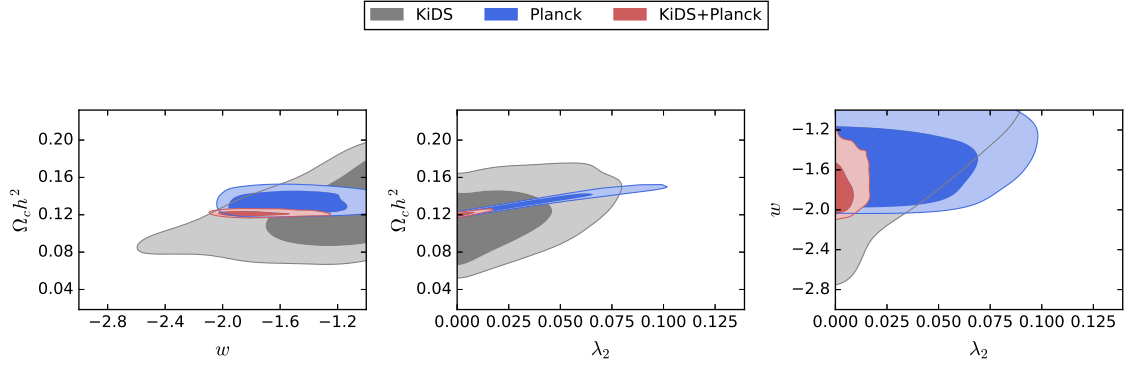


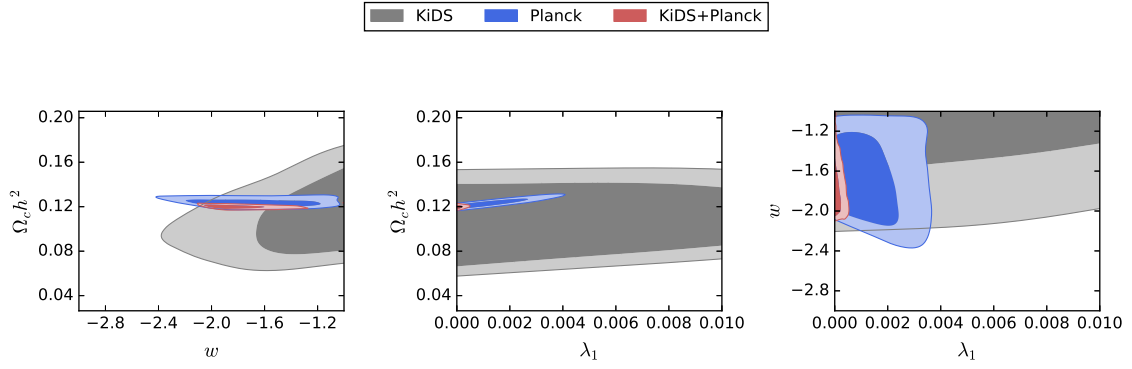
FIG. 4: 1D likelihood functions for selected parameters



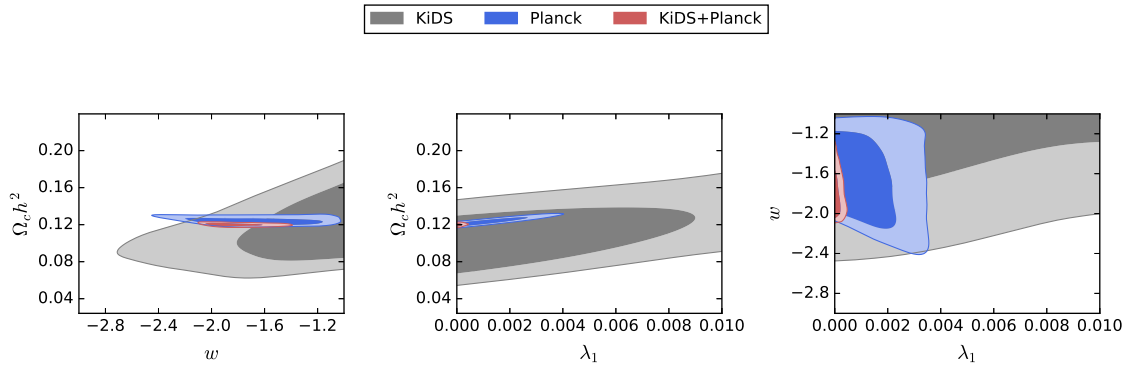
(a) Model I



(b) Model II



(c) Model III



(d) Model IV

FIG. 5: 2D posterior contours for selected parameters